Phase-space signatures of the Anderson transition

André Wobst,[1] Gert-Ludwig Ingold,[1] Peter Hänggi,[1] and Dietmar Weinmann[2]
[1]*Institut für Physik, Universität Augsburg, Universitätsstraße 1, D-86135 Augsburg, Germany*
[2]*Institut de Physique et Chimie des Matériaux de Strasbourg, UMR 7504 (CNRS-ULP), 23 rue du Loess, BP 43, F-67034 Strasbourg Cedex 2, France*
(Received 14 March 2003; published 7 August 2003)

We use the inverse participation ratio based on the Husimi function to perform a phase-space analysis of the Anderson model in one, two, and three dimensions. Important features of the quantum states remain observable in phase space in the large system size limit, while they would be lost in a real- or momentum-space description. From perturbative approaches in the limits of weak and strong disorder, we find that the appearance of a delocalization-localization transition is connected to the coupling, by a weak potential, of momentum eigenstates which are far apart in momentum space. While this is fully consistent with the known dependence of the existence of the Anderson transition on dimensionality, the resulting criterion can be applied to other models as well. The phase-space approach thus sheds new light on the metal-insulator transition.

DOI: 10.1103/PhysRevB.68.085103 PACS number(s): 71.23.An, 05.60.Gg, 05.45.Pq

I. INTRODUCTION

Phase-space concepts are widely used in various areas of physics like quantum optics[1] and quantum chaos,[2,3] while they are rarely employed in condensed matter physics. In this work, we use a phase-space analysis to address the Anderson metal-insulator transition, and demonstrate that such a description is very useful and represents a powerful tool to describe and to elucidate how, as a function of a parameter, the nature of the eigenstates changes from delocalized to localized.

While delocalized states call for a description in terms of momentum eigenstates, in particular in the ballistic regime, real-space methods are expected to be appropriate in the localized regime. Even though the real-space wave function in itself contains already the full information about a quantum state, a phase-space representation may be much better suited to display the relevant information, e.g., in the vicinity of a delocalization-localization transition, where both real-space and momentum-space features are expected to play an important role.

The relevance of a phase-space description has recently been illustrated by comparing the one-dimensional Anderson model and the Aubry-André model. In the first case, already the presence of very weak disorder leads to localized states in the thermodynamic limit.[4] In the quasiperiodic potential of the Aubry-André model, however, a localization transition occurs at a critical potential strength.[5] From a phase-space analysis, it was concluded that this qualitative difference between the two one-dimensional models is due to the very different couplings of the momentum eigenstates, induced by the disorder and the quasiperiodic potential, respectively.[6]

In this work, we study the phase-space behavior of the Anderson model in one, two and three dimensions and show that the above considerations are not restricted to one-dimensional models. Conversely, it turns out that the proposed relation between the coupling of momentum eigenstates due to a weak potential and the occurrence of a metal-insulator transition allows to explain why the Anderson transition cannot occur in one dimension.

In view of the wealth of known results,[7] the Anderson model is particularly well suited for this kind of study. First studies of the one- and two-dimensional Anderson model based on the Wehrl entropy[8,9] had already demonstrated that the diffusive regime present in two dimensions becomes apparent in phase space.[10] An extension to the three-dimensional Anderson model has become possible by calculating inverse participation ratios in phase space instead of entropies.[11] Using the phase-space analysis, we recover that in the thermodynamic limit all states are localized in one dimension, while two dimensions represent the marginal case. In three and higher dimensions, the phase-space behavior provides clear signatures of the Anderson transition where states become localized only above a critical disorder strength.[12] This allows one to gain a detailed understanding of the phase-space concepts and opens the road towards their application to more complicated systems.

In Sec. II we start by introducing the characterization of quantum states by their inverse participation ratio (IPR) in phase space as well as the corresponding quantities in real and momentum space. The Anderson model is introduced in Sec. III, and numerical results for its phase-space behavior in the whole range from the ballistic to the localized regime are presented in Sec. IV. The observed features are discussed in the light of known properties of the eigenstates. Since the behavior in the limiting cases of weak and strong disorder turns out to depend on the dimensionality and to be indicative of the existence of a metal-insulator transition, we devote the main part of this paper to a detailed investigation of these limits. Perturbative expansions for the inverse participation ratios in the different spaces are presented for strong disorder in Sec. V A and for the limit of weak disorder in Sec. V B. Here, a crucial dependence of the inverse participation ratio on dimension is identified, and related to the structure of the coupling of momentum eigenstates by weak disorder. This important property is only apparent in phase space while such signatures cannot be extracted from the inverse participation ratios neither in real nor momentum space. Our interpretation and the relation to the known properties of the Anderson model, in particular in the marginal

case of two dimensions, is confirmed by an analysis of the dependence of the inverse participation ratio on system size in Sec. VI. Finally, we present our conclusions in Sec. VII.

II. CHARACTERIZATION OF STATES

Among the infinite variety of possible phase-space representations of a quantum state,[13] the Husimi[14] or Q function[15] is best suited for our purpose because it guarantees a positive definite density. This property will allow us to define an inverse participation ratio in Eq. (3) below. The positivity is a direct consequence of the definition of the Husimi function

$$\rho(\mathbf{x}_0,\mathbf{k}_0)=|\langle \mathbf{x}_0,\mathbf{k}_0|\psi\rangle|^2, \tag{1}$$

where the state $|\psi\rangle$ is projected onto a minimal uncertainty state $|\mathbf{x}_0,\mathbf{k}_0\rangle$ centered around position $\mathbf{x}_0$ and momentum $\mathbf{k}_0$ in phase space. The minimal uncertainty state assumes a Gaussian form both in position and momentum representation. Its real-space wave function reads

$$\langle \mathbf{x}|\mathbf{x}_0,\mathbf{k}_0\rangle=\left(\frac{1}{2\pi\sigma^2}\right)^{d/4}\exp\left(-\frac{(\mathbf{x}-\mathbf{x}_0)^2}{4\sigma^2}+i\mathbf{k}_0\cdot\mathbf{x}\right). \tag{2}$$

In the definition (1) of the Husimi function, the width σ appearing in Eq. (2) determines the relative importance of structures in real and momentum space. We adopt this definition for lattice models with periodic boundary conditions provided that $\sigma \ll L$. Here, L is the number of lattice sites in one spatial direction and the lattice constant sets the unit length. Throughout this paper, we choose $\sigma=\sqrt{L/4\pi}$ which yields an equal width of the Gaussian relative to the system size L and the momentum interval running from $k=-\pi$ to π.

Since we are ultimately interested in the thermodynamic limit, $L\to\infty$, let us first discuss the dependence on system size of the phase-space resolution provided by the Husimi function. Since the d spatial components are independent of each other, it is sufficient to consider the one-dimensional case. For our choice of σ, the Gaussian smearing arising from the projection onto a minimal uncertainty state affects areas in phase space which contain a number of grid points that is of the order of $\sqrt{L}\times\sqrt{L}$. Structures appearing on smaller scales cannot be resolved. However, even though the absolute resolution degrades, relative to the size of the system the resolution becomes increasingly better as the system size is increased. This holds for any σ which scales with system size like L^α where $0<\alpha<1$. In contrast, the limiting cases $\alpha=0$ and $\alpha=1$ behave quite differently. For $\alpha=0$, we have optimal resolution in real space but cannot resolve phenomena in momentum space, even in the thermodynamic limit. The opposite is true for $\alpha=1$ where one would obtain a pure momentum-space description. Our choice of $\alpha=1/2$ leads to an ideal balance between these two extreme cases, and allows one to track features to the thermodynamic limit which rely on both real and momentum space.

The Husimi function contains a tremendous amount of information about a quantum state. It turns out, however, that relevant information can already be extracted by considering the inverse participation ratio in phase space,[11]

$$P=\sum_{\mathbf{x},\mathbf{k}}\frac{1}{L^d}[\rho(\mathbf{x},\mathbf{k})]^2, \tag{3}$$

where the sum runs over all phase-space points $(\mathbf{x},\mathbf{k})$. The normalization in Eq. (3) is chosen in such a way that $P=1/2$ corresponds to an optimal localization around one lattice point. In phase space, this is achieved by a minimal uncertainty state. A distribution of the Husimi density over a larger volume in phase space corresponds to lower values of P.

Although the IPR in phase space (3) is defined in terms of the Husimi function $\rho(\mathbf{x},\mathbf{k})$, it may be calculated directly from the wave function,[11,16,17] by means of a straightforward generalization of the one-dimensional expression given in Refs. 11 and 16. Such an approach provides significant numerical advantages and is crucial for the treatment of higher-dimensional systems.

The IPR in phase space P should be compared with the IPR in real space which has frequently been employed to describe quantum states in disordered systems.[18–21] Here, the state $|\psi\rangle$ is projected onto a Wannier state $|\mathbf{x}\rangle$ localized on a single site of the lattice. This allows one to define the IPR in real space as

$$P_x=\sum_{\mathbf{x}}|\langle\psi|\mathbf{x}\rangle|^4, \tag{4}$$

which corresponds to the limit $\sigma\to 0$ of the IPR in phase space. It is also convenient to introduce the IPR in momentum space as

$$P_k=\sum_{\mathbf{k}}|\langle\psi|\mathbf{k}\rangle|^4, \tag{5}$$

where the basis of momentum eigenstates $|\mathbf{k}\rangle$ is given by $\langle\mathbf{x}|\mathbf{k}\rangle=\exp(i\mathbf{k}\cdot\mathbf{x})/L^{d/2}$.

As will be seen below, even the combined information from the IPRs in real and momentum-space is not equivalent to the information provided by the IPR in phase space. However, it was shown in Ref. 22 that by an appropriate Gaussian smearing of the real- and momentum-space densities one can define marginal distributions which allow one to reproduce the behavior of the IPR in phase space. Unfortunately, this approach does not result in a reduction of the numerical effort as compared to the calculation of the IPR in phase space.

III. ANDERSON MODEL

In the following, we shall present a detailed comparison of the IPRs in real, momentum, and phase space by considering the Anderson model for a quantum particle in a disordered potential. Its Hamiltonian

$$H=-t\sum_{\langle\mathbf{x},\mathbf{x}'\rangle}(|\mathbf{x}'\rangle\langle\mathbf{x}|+|\mathbf{x}\rangle\langle\mathbf{x}'|)+W\sum_n v_n|\mathbf{x}\rangle\langle\mathbf{x}| \tag{6}$$

is defined on a d-dimensional square lattice with L sites in each direction. The energy scale is set by the hopping matrix elements $t=1$ between nearest neighbor sites $\langle\mathbf{x},\mathbf{x}'\rangle$. In order to avoid boundary effects we choose periodic boundary

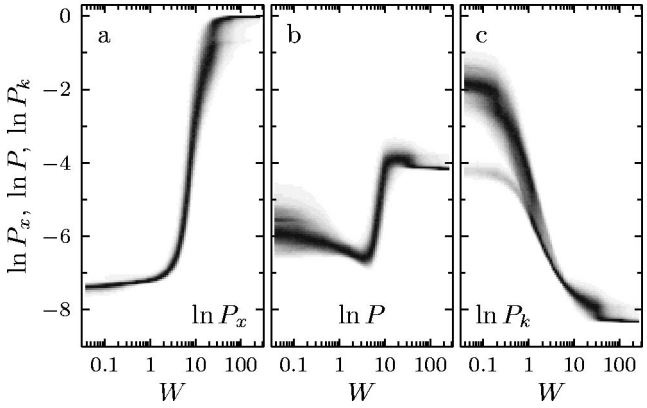

FIG. 1. Gray scale plot for the distributions of the logarithms of the inverse participation ratios in (a) real space, (b) phase space, and (c) momentum space as a function of the disorder strength W. The data represent $L^2/2$ states around the band center, for 50 different disorder realizations of the two-dimensional Anderson model of size $L=64$.

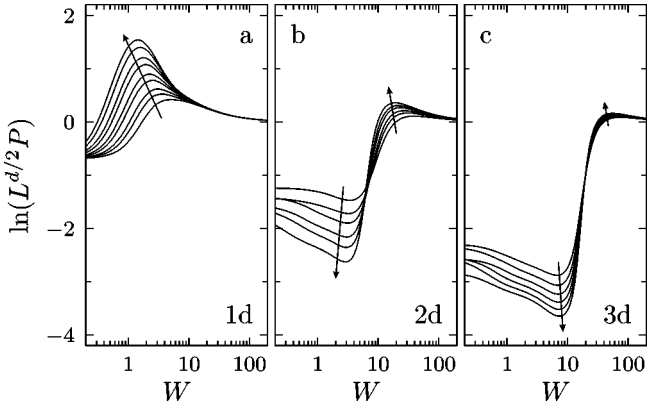

FIG. 2. Mean IPR in phase space as a function of the disorder strength for (a) one, (b) two, and (c) three dimensions for system sizes (a) $L=128$, 192, 256, 384, 512, 768, 1024, 1536, and 2048; (b) $L=16$, 24, 32, 48, 64, and 96; (c) $L=14$, 16, 18, 20, 22, and 24. The arrows indicate how the position W of the extrema shifts with increasing L.

conditions in each direction so that every site has $2d$ nearest neighbors. The on-site energies v_n forming the disordered potential are drawn independently from a box distribution on the interval $[-1/2;1/2]$ and W denotes the disorder strength.

The structure of the quantum eigenstates of the Anderson model depends on the disorder strength. For vanishing disorder, the eigenstates are plane waves and thus are localized in momentum space. In the opposite limit of strong disorder, localization in real space takes place. In order to describe the behavior of the states in the whole parameter region, and in particular the transition between the limiting regimes, it is very useful to work with phase-space quantities which adequately take into account real-space as well as momentum-space properties at the same time.

IV. INVERSE PARTICIPATION RATIOS FOR THE ANDERSON MODEL

In order to appreciate the advantage of the phase-space approach, we start by comparing the IPR's in real space, P_x, phase space, P, and momentum space, P_k, for the two-dimensional Anderson model. In Fig. 1, numerical results are shown for a lattice of size 64×64. For each given disorder strength W, we have diagonalized Hamiltonian (6) for 50 different disorder realizations $\{v_n\}$, and used $L^2/2$ states around the band center to calculate distributions of logarithms of the IPRs.

In Fig. 1(a) we observe a monotonic increase of the real-space IPR with increasing disorder strength W. This corresponds to the tendency towards localization of the eigenfunctions. According to Fig. 1(c), the IPR in momentum space simultaneously decreases, thereby indicating delocalization in momentum space. This behavior of P_x and P_k is an immediate consequence of the system's change from the ballistic regime for weak disorder, e.g., localization in momentum space, to localized states in real space for strong disorder.

Since the IPRs in real and momentum space evolve in opposite directions as a function of the disorder strength, the behavior of the phase-space IPR, which describes the spread of the wave function in real and momentum space on an equal footing, can be expected to provide more subtle information. Indeed, the behavior of the phase-space IPR depends on the details of the model, as can be seen by a comparison of the one-dimensional Anderson model and the Aubry-André model,[6] and within the Anderson model itself, where the dimensionality plays a crucial role.[11]

For the two-dimensional case, the IPR in phase space depicted in Fig. 1(b) displays a much richer structure than the IPRs in real and momentum space. In particular, the dependence on the disorder strength W is nonmonotonic, and one finds a minimum at an intermediate value of W which can be associated with diffusive behavior.[11] This nontrivial behavior motivates the following in-depth study of the Anderson model by means of the IPR in phase space.

Figures. 2(a)–2(c) depict the mean IPR in phase space for one, two, and three dimensions, respectively, for various system sizes L. The arrows indicate the shift of the extrema with increasing system size. The data have been scaled with the length dependence $L^{-d/2}$ of the limiting cases at $W=0$ and $W\to\infty$, cf. Sec. V. Before giving a detailed discussion of the dependence on L in Sec. VI, we concentrate on the overall behavior as a function of the disorder strength.

One of the most striking aspects of the results presented in Figs. 2(a)–2(c) is that the behavior of the phase-space IPR at weak disorder depends on the spatial dimension in a crucial way. While in $d=1$ the IPR increases with increasing W, it decreases in $d\geqslant 2$. Together with the fact that, independently of the dimension d, at strong disorder the limiting value for $W\to\infty$ is approached from above, this has important consequences for the global behavior of the phase-space IPR. In $d=1$, the two limits are joined by a peak indicating localization in phase space. In contrast, in two and three dimensions, P decreases in the regime of small disorder, and assumes a minimum indicating a large spreading in phase space followed by a more or less steep rise towards a maximum, as can be seen in Figs. 2(b) and 2(c).

The minimum of the phase-space IPR in two and higher

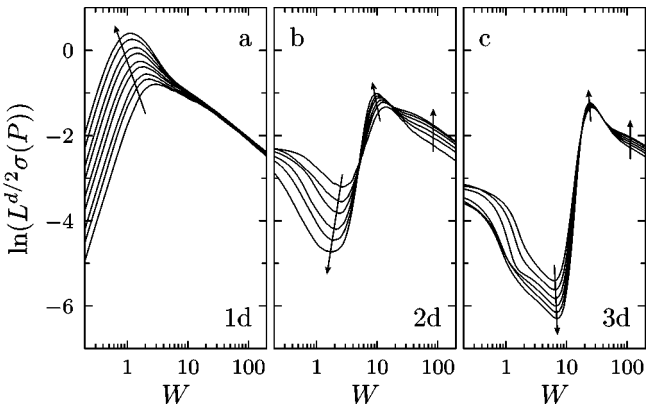

FIG. 3. The standard deviation $\sigma(P)$ of the IPR in phase space as a function of the disorder strength for (a) one, (b) two, and (c) three dimensions and the same parameters as in Fig. 2.

dimensions can be associated with the existence of a diffusive regime where the system size is much larger than the mean free path but smaller than the localization length. The resulting mixing of the plane waves by the disorder potential considerably alters the structure of the states and leads to a spreading both in real and momentum space and thus to a small value of the phase-space IPR. This is reminiscent of the emergence of quantum chaos and can be confirmed by determining the energy level statistics around the minimum of P. One indeed finds Wigner-Dyson statistics[11] which characterizes the diffusive (chaotic) regime.

In addition to the mean value, the distribution of the phase-space IPR at given disorder strength [cf. Fig. 1(b) for the case $d=2$] can be characterized by the standard deviation $\sigma(P)$ depicted in Fig. 3 for one, two, and three dimensions. Here, we have employed the same scaling with system size as in Fig. 2. The overall structure resembles the one found for the mean values. The strong suppression of the standard deviation occurring in the diffusive regime, being particularly pronounced in $d=3$, indicates that the phase-space structure is quite independent of the individual states. This confirms once more the universal chaotic character of the diffusive states which is expected due to the strong mixing present in this regime.

V. PERTURBATION THEORY

The numerical results for the phase-space IPR presented in Figs. 2 and 3 indicate that the changes in the global behavior as a function of the disorder strength can be understood in terms of the limiting behavior for strong disorder and, in particular, for weak disorder. Therefore, we proceed next to a detailed perturbative investigation of the IPRs in these two limits. We start with the simpler case given by the limit of strong disorder.

A. IPR at strong disorder

For $W\to\infty$, all eigenstates are localized on single sites in real space. A finite ratio t/W then leads to a coupling to the nearest neighbor sites due to the kinetic energy in Eq. (6). Such a perturbation can be treated analytically as long as it is sufficient to take into account only the coupling to the nearest neighbor state which is closest in energy to the initial site. For the resulting two state system, the IPRs may be calculated explicitly. The other nearest neighbor sites enter in the calculation only when the disorder average is performed.

In a first step, we thus focus on two nearest neighbor Wannier states on a lattice of size L^d. The absolute value of the difference between the corresponding on-site energies will be denoted by Δ. Then the effective Hamiltonian for the two level system in the Wannier basis reads

$$H_{\mathrm{TLS}}=\begin{pmatrix} -\Delta/2 & -t \\ -t & \Delta/2 \end{pmatrix}. \tag{7}$$

It is straightforward to determine the two eigenstates and the corresponding IPRs, which are identical for both states. Introducing the eigenenergies $\tilde{\Delta}=\pm[(\Delta/2)^2+t^2]^{1/2}$, the IPRs are given by

$$P_x(\Delta)=1-\frac{t^2}{2\tilde{\Delta}^2},$$

$$P_k(\Delta)=L^{-d}\left[1+\frac{t^2}{2\tilde{\Delta}^2}\right], \tag{8}$$

$$P(\Delta)=L^{-d/2}\left[1+\frac{t^2}{2\tilde{\Delta}^2}[2\exp(-1/4\sigma^2)-1]\right].$$

In particular, one finds $P_x(0)=1/2$ because for degenerate on-site potentials the two states are both equally distributed over the two sites. Furthermore, and consistent with the results of Sec. IV, the IPRs in real and momentum space behave oppositely as t/W is increased. For a large system size, the IPR in phase space increases with t/W, just as the IPR in momentum space.

In order to compare with our numerical results, we need to perform a disorder average. Since the on-site energies are equally distributed inside the interval $[-W/2;W/2]$, the probability density p_1 that two neighboring on-site energies differ by Δ reads

$$p_1(\Delta)=\frac{2}{W^2}(W-\Delta). \tag{9}$$

The index 1 indicates that only one nearest neighbor site is taken into account.

Furthermore, we need to ensure that the energy difference Δ is the smallest among the energy differences with all nearest neighbors. Therefore, for the remaining $2d-1$ nearest neighbors, the difference in on-site energy with respect to the central site should be larger than Δ. The probability density for such a $2d$ nearest neighbor configuration is given by

$$p_{2d}(\Delta)=N^{-1}p_1(\Delta)\left(\int_\Delta^W dx p_1(x)\right)^{2d-1}$$

$$=4d\left(1-\frac{\Delta}{W}\right)^{4d-1}, \tag{10}$$

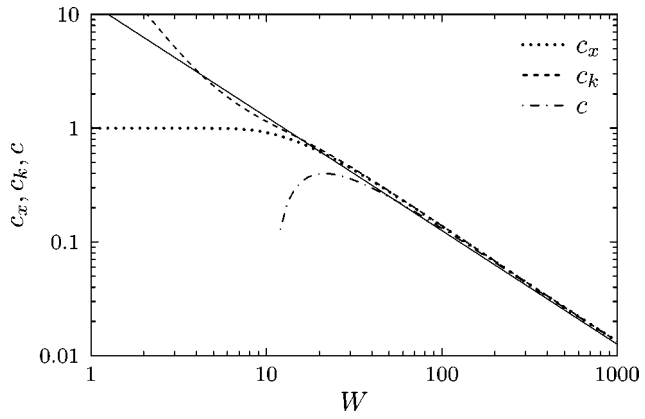

FIG. 4. Comparison of the perturbative result $2\pi d(t/W)$ (solid line) with the numerically computed values for deviations of the IPRs from their value at $W=\infty$ in real space (c_x, dotted line), momentum space (c_k, dashed line), and phase space (c, dashed-dotted line), for the parameters of Fig. 1.

where N is a normalization constant.

Within the assumption that we can restrict ourselves to an effective two level system, we therewith obtain the IPR in phase space,

$$P=\int_0^W d\Delta p_{2d}(\Delta)P(\Delta) \tag{11}$$

together with corresponding expressions for the IPRs in real and momentum space. Making use of Eq. (8) and (10), to leading order in t/W, one obtains

$$P_x=1-2\pi d\frac{t}{W},$$

$$P_k=L^{-d}\left(1+2\pi d\frac{t}{W}\right), \tag{12}$$

$$P=L^{-d/2}\left(1+2\pi d\frac{t}{W}[2\exp(-1/4\sigma^2)-1]\right),$$

with corrections of order $(t/W)^2\ln(t/W)$. Configurations where more than one nearest neighbor site is energetically degenerate with the central site do not modify results (12) because the probability to find such a configuration vanishes.

In order to compare the numerical data presented in Fig. 1 with the perturbative result, we introduce the quantities $c_x=1-P_x$, $c_k=L^dP_k-1$, and $c=(L^{d/2}P-1)/[2\exp(-1/4\sigma^2)-1]$. Within the perturbative results of Eq. (12), we have $c_x=c_k=c=2\pi d(t/W)$. The numerical results for the two-dimensional Anderson model are shown in Fig. 4. The agreement with the leading perturbative results is remarkably good for disorder strengths down to rather small values of W. This is particularly true for the IPR in momentum space represented by the dashed line. The fact that IPRs are by definition positive quantities implies that the correction c_x of the IPR in real space depicted by the dotted line is limited from above by 1. Therefore, the leading correction to P_x given by Eq. (12) must fail when c_x reaches this limiting value. Finally, the dash-dotted line corresponding to the phase-space term c is well described by the leading perturbative correction according to Eq. (12) down to $W\approx 30$ for this system of 64×64 sites.

As for the case of two sites, Eq. (8), the IPRs in real and momentum space move in the opposite direction as a function of t/W. Moreover, the IPR in phase space still behaves similarly to the momentum-space IPR, for the averaged quantities given by Eq. (12). The key to an understanding of this behavior of the IPR in phase space lies in the limited resolution provided by the Husimi function. Since its spatial resolution is of order $L^{1/2}$, changes which occur only on two lattice sites will not affect the Husimi functions, in particular in the case of large system sizes. Only the small deviation of the factor $2\exp(-1/4\sigma^2)-1$ from 1 can be traced back to real-space behavior as an incomplete overlap of the Gaussians centered at the two sites in question. Small scale changes in real space, however, lead to large scale changes in momentum space. In the regime discussed above, one observes beatings in the momentum-space density as a consequence of the required orthogonality of the two eigenstates of Eq. (7). This effect can be resolved by the Husimi function, so that momentum-space effects dominate the phase-space behavior at strong disorder.

Finally, the difference of $L^{d/2}$ in the prefactor of the IPRs in phase space and momentum space stems from the Gaussian smearing in phase space which contributes, in our case of spatially well-localized states, a factor $\sigma\propto L^{1/2}$ for each spatial dimension.

B. IPR at weak disorder

As shown in Fig. 1, the IPRs in real and momentum space exchange their qualitative role as compared to the strong disorder limit. This is not surprising, because ballistic motion of a quantum particle implies the existence of plane waves with well localized momentum and delocalization in real space. Exchanging real and momentum space, this corresponds to the real-space scenario for strong disorder.

The situation, however, is more complicated in phase space, and the behavior in the limit of weak disorder, $W\rightarrow 0$, is by far more complex. Only in one dimension, the IPR in phase space can indeed be understood in terms of the real-space IPR at weak disorder and the momentum-space IPR at strong disorder.[11] In particular, the IPR in phase space increases with increasing disorder strength in the regime of weak disorder. The scenario, however, is very different for two and higher dimensions as can already be seen from Fig. 1(b) where the phase-space IPR displays a decrease at weak disorder. In this case, the momentum-space behavior dominates the phase-space IPR at both weak and strong disorder. Examples of IPRs in real, momentum, and phase space in dimensions up to $d=3$ are given in Fig. 4 of Ref. 23. In the following, we will distinguish the cases $d=1$ and $d\geqslant 2$.

1. IPR at weak disorder for $d=1$

First, we briefly review the phase-space properties of the one-dimensional Anderson model, which were already discussed in Refs. 11 and 6 in some detail. For $W=0$, two plane

waves at momentum values k and $-k$ are energetically degenerate, and there is an ambiguity in the choice of the corresponding two basis states. We choose symmetric and antisymmetric combinations of the two plane waves, in order to obtain real wave functions. The solutions in the limit $W \to 0$ singled out by degenerate perturbation theory contain additional phases which, however, do not influence any of the discussed IPRs.

In the clean case, $W=0$, one finds $P_k=1/2$ for states with nonvanishing momentum. This corresponds to the equally weighted contribution of the two momenta k and $-k$. In real space, the sum appearing in the IPR can be approximated by an integral and it is sufficient to consider as a representative the wave function $\sqrt{2/L}\cos(kx)$. This yields, for the IPR in real space,[26]

$$\int_0^L dx \left(\sqrt{\frac{2}{L}} \cos(kx) \right)^4 = \frac{3}{2L}. \tag{13}$$

In phase space the Husimi function resolves the two momenta k and $-k$ which are well separated for energies around the band center. While for $W \to \infty$ a single stripe in phase space leads to an inverse participation ratio $L^{-1/2}$, the two stripes now result in $L^{-1/2}/2$.

The presence of a disorder potential leads to a coupling of plane waves with different momenta. In contrast to the opposite case of strong disorder, $W \to \infty$, where the coupling of the Wannier states occurs only between neighboring sites, for weak disorder $W \to 0$, the coupling of the plane waves is not restricted to neighboring momenta. In fact, the averaged matrix element of the disorder potential is independent of the momenta of the states involved. Within perturbation theory, however, the energy difference of the states comes into play so that effectively the coupling to states close in energy (but not necessarily in momentum) is dominant.

Only for the one-dimensional case does the dispersion relation $E=-2t\cos k$ imply, that real basis states at $W=0$ which are close in energy E are also close in momentum k. As a consequence, only states which are close in momentum are efficiently coupled by a weak disorder potential. Although the perturbative treatment is more complicated for weak than for strong disorder, a qualitative impression of its effect on the phase-space properties can be obtained in analogy to the case $W \to \infty$ by interchanging real and momentum space. Now, because of the limited resolution of the Husimi function, the coupling to close states in momentum space does not have a significant effect while the large scale modulation in real space associated with the coupling affects the Husimi function. Therefore, while the value of the IPR in phase space for a clean one-dimensional Anderson model at $W=0$ is a direct consequence of the localization in momentum space, the corrections for finite $W \to 0$ are dominated by real-space effects.

2. IPR at weak disorder for d≥2

Generic ballistic states on a d-dimensional cubic lattice display a $2^d d!$-fold energetic degeneracy. The factor 2^d arises from the degeneracy between momentum vectors with different signs of the components, while the factor $d!$ accounts for the number of possible permutations of a set of d momentum values, provided they are all different. For example, in three dimensions all eight different combinations of the signs in $\mathbf{k}=(\pm k_1, \pm k_2, \pm k_3)$, and all six permutations of the momentum components $\{k_1, k_2, k_3\}$ lead to the same energy $E=-2t(\cos k_1+\cos k_2+\cos k_3)$. Occasionally, the degeneracies may even be larger. This is the case when the same total energy can be achieved by different sets of momentum components.

While for two degenerate states the limit $W \to 0$ leads to a universal value for the IPRs, this is no longer true in the case of higher degeneracies, where the IPRs depend on the disorder realization, even in the limit $W \to 0$. This can already be seen from the existence of different types of (real) wave functions. An optimal localization in momentum space can be obtained by pairing only two plane waves with opposite momenta $\mathbf{k}$ and $-\mathbf{k}$, leading to

$$\psi(\mathbf{x}) = (2/L)^{d/2} \cos(\mathbf{k}\cdot\mathbf{x}). \tag{14}$$

A wide distribution in momentum space is achieved by a linear combination of all energetically degenerate states. For a generic state this yields

$$\phi(\mathbf{x}) = \frac{1}{(2^{d-2} d! L^d)^{1/2}} \sum_{P(\{k_i\})} \sum_{\{\eta\}} \cos\left(\sum_{i=1}^{d} \eta_i k_i x_i \right), \tag{15}$$

where the first sum is to be taken over all permutations of the set of (different) momentum components k_i while the second sum over the set of η_i is to be taken over all combinations of factors ± 1 with $\eta_1=+1$ kept fixed. Only for $d=1$ the states $\psi(x)$ and $\phi(x)$ coincide, again hinting at the difference between the weak disorder behavior in one dimension and the subtleties appearing in higher dimensions.

It follows that in two and higher dimensions a nontrivial distribution of IPRs already appears in the limit $W \to 0$. Figure 5 depicts such distributions for a set of eightfold degenerate states in two dimensions with momentum components $\pm 5\pi/24$ and $\pm 3\pi/4$. The system size of $L=48$ ensures that the overlap of the Husimi functions corresponding to the eight different momentum vectors is negligible.

The two states (14) and (15) help to understand the distribution for the momentum-space IPR. On the one hand, $\psi(\mathbf{x})$ yields the maximum IPR in momentum space for real wave functions, $P_k=1/2$. On the other hand, all plane waves might be equally weighted as in state $\phi(\mathbf{x})$, thus leading to an inverse participation ratio of 1/8 in momentum space. It turns out that the mixing of the plane waves due to a random potential is quite efficient, thus making the first limit rather improbable.

For the case presented in Fig. 5, the two momentum components k_1 and k_2 are well separated on the scale of the phase-space resolution in momentum direction $\sqrt{\pi/L}$. Consequently, the overlap of the resulting stripes in phase space is negligible. Therefore, the distributions for the IPR in momentum space and phase space coincide up to a scaling fac-

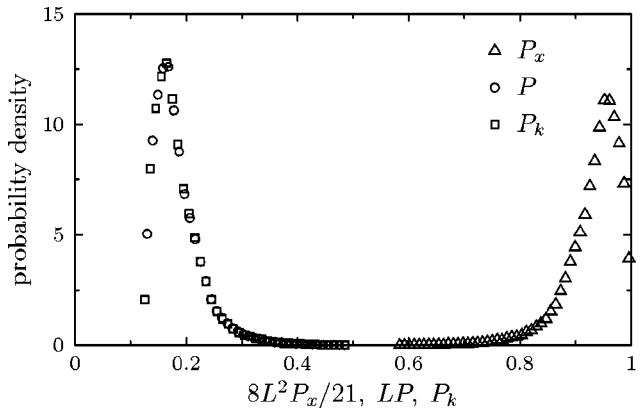

FIG. 5. Distributions of the IPRs in real space (triangles), phase space (circles), and momentum space (squares) in the zero disorder limit $W\rightarrow 0$. A generic set of eightfold degenerate states in two dimensions with momentum components $\pm 5\pi/24$ and $\pm 3\pi/4$ is considered for a system of size $L=48$ where the overlap of the Husimi functions for stripes at k_1 and k_2 is negligible. The distributions are obtained by taking all eight degenerate states for 10 000 disorder realizations into account.

tor $L^{-d/2}$ which arises from the finite width of the Husimi function in the d momentum directions.

In contrast to the behavior in momentum and phase space, an equally weighted combination of all energetically degenerate plane waves leads to a maximum of the IPR in real space. For every pair of different and nonzero momentum components k_1 and k_2, which are both a multiple of $2\pi/L$, the IPR for such a state becomes, in an integral approximation,

$$P_x=\int_0^L d\mathbf{x}\ \phi(\mathbf{x})^4=\frac{21}{8L^2}. \tag{16}$$

When only one momentum direction contributes, the opposite limit is reached, and the IPR in real space becomes

$$P_x=\int_0^L d\mathbf{x}\ \psi(\mathbf{x})^4=\frac{3}{2L^2}, \tag{17}$$

which, up to a factor $1/L$, coincides with the result in one dimension, cf. Eq. (13). Since the equally weighted states described by Eq. (15) now lead to larger values of the IPR, the result in real space is essentially a mirror image of the IPRs in momentum and phase space (see Fig. 5).

In three dimensions the IPRs for a generic situation of 48-fold degeneracy may be obtained as well. While $L^{3/2}P$ and P_k yield values between 1/48 and 1/2, the IPR in real space assumes values between $3/2L^3$ and $61/16L^3$. The latter values are obtained by a calculation analogous to that underlying Eqs. (16) and (17).

We emphasize once more that the states discussed above represent the generic states. In addition, there exist states where some or all of the momentum components are equal so that the number of degenerate states is decreased. On the other hand, in certain cases a given total energy can be constructed by different sets of momentum components thus giving rise to an increase of the degeneracy. These special states are relevant for a detailed description of the complete distribution of IPRs for a given system size, which may exhibit a complex structure. However, in the limit of large system size, the generic states discussed above dominate the distributions.

From the perturbative investigation of the IPR in the limits of very strong and very weak disorder, we can conclude that real-space properties will only dominate at weak disorder strength, if a coupling is induced predominantly between plane waves close in momentum. As long as the distance in momentum is below the momentum uncertainty $\sqrt{\pi/L}$ in phase space, such a coupling will become apparent only via the large scale real-space structure appearing in the Husimi function. Therefore, in this scenario which is characteristic for one dimension, real space dominates at weak disorder strength and the phase-space IPR increases with increasing disorder. It is only the value of $P(W=0)$ itself which is determined by momentum-space properties.

In two and higher dimensions the picture changes drastically, because states close in energy are not necessarily close in momentum anymore. In this case, the disorder potential may scatter plane waves into other momentum directions and thus induces a strong mixing in momentum space. In particular, states of the type of Eq. (14), which yield large values for P, are affected by such processes. The mixing will thus lead to a decrease of the IPR in phase space as a consequence of the dominance of momentum space. In contrast, the real-space structure will appear on relatively small length scales which are typically not resolved by the Husimi function. As we will see in Sec. VI, this decrease of P in $d\geqslant 2$ implies the existence of a regime of intermediate disorder where phase space is well covered by the Husimi function and which can be associated with diffusive behavior. Furthermore, this scenario opens the possibility of a delocalization-localization transition.

VI. SYSTEM SIZE DEPENDENCE

While the Anderson model in three dimensions exhibits a phase transition from delocalized states at weak potential to localized states at strong potential, such a phase transition is absent for the Anderson model in two dimensions, where all states are localized in the thermodynamic limit. Nevertheless, for a fixed system size, both models show qualitatively the same behavior of the IPR in phase space, calling for an analysis of the size dependence of the IPR in order to check whether or not the strong increase of the phase-space IPR at the crossover between the diffusive and the localized regime evolves towards an abrupt jump which would indicate a phase transition in the limit $L\rightarrow\infty$.

To this end we plot in Fig. 6, versus the system size L, the disorder strengths W at which for the Anderson model in one, two and three dimensions maxima and minima of the phase-space IPR occur. The locations of minima and maxima are shown as open and full symbols, respectively. While scaling laws cannot be extracted from the data,[27] one can nevertheless clearly observe the direction of the shift of minima and maxima as a function of the system size. This reveals an important difference between the cases of two and three di-

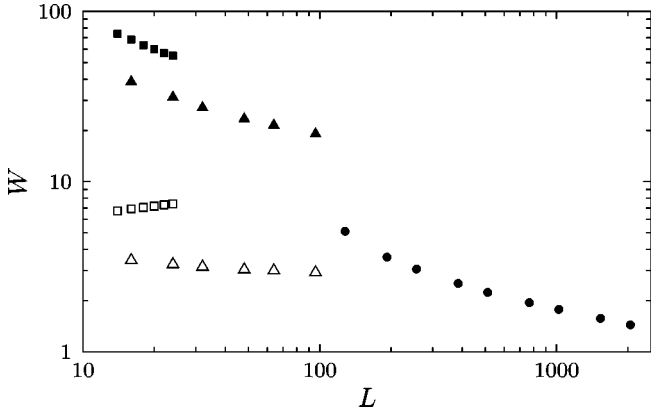

FIG. 6. Values of the disorder strength W for the minima (open symbols) and maxima (full symbols) of the inverse participation ratio in phase space, as a function of the system size. The circles, triangles, and squares are for one, two, and three dimensions, respectively.

mensions. In three dimensions, the position of the maximum moves to lower disorder values when the system size is increased, while the position of the minimum shifts in the opposite direction. From this trend, one can expect that in the limit $L\to\infty$, the positions of the maximum and the minimum converge towards the same finite disorder value, with the emergence of a nonmonotonic step in the disorder-dependence of the phase-space IPR as a clear signature of the Anderson transition in phase space.

In order to get an estimate of the critical disorder strength W_c for the Anderson model in $d=3$, in Fig. 7 we depict the change of the phase-space IPR as a function of the system size for fixed values of the disorder strength. For $W<W_c$, the phase-space IPR should decrease with increasing L while for $W>W_c$ it increases. For $W=19.1$ (indicated by circles), P will increase with the system size. For $W=17.4$ (squares), P decreases for the system sizes accessible to us, but one may anticipate that the curve will rise for larger system sizes. Such a behavior can also be observed for the two-

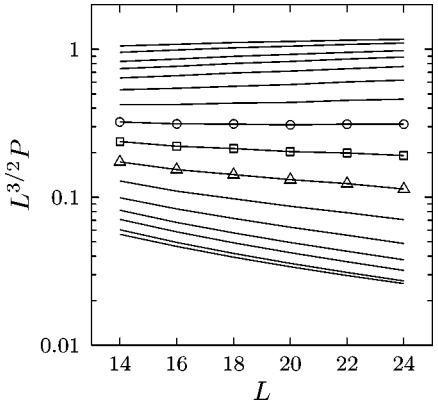

FIG. 7. Dependence of the phase-space IPR on the system size for the Anderson model in $d=3$ at fixed disorder strengths $W=6.9$, 9.1, 11.0, 12.0, 13.2, 14.5, 15.8 (triangles), 17.4 (squares), 19.1 (circles), 20.9, 22.9, 25.1, 27.5, 30.2, 36.3, and 47.9 from the lower to the upper curve.

dimensional Anderson model. In contrast, for $W=15.8$ (triangles), one would expect that the curve continues to fall even for larger system sizes. This implies a critical value for the disorder strength between 15.8 and 17.4. While these considerations are not necessarily stringent, the results presented in Fig. 7 as well as in Figs. 2 and 6 are perfectly consistent with the known value of $W_c\approx 16.5$ for the Anderson transition in the band center.[24]

In contrast, according to the data depicted in Fig. 6 for two dimensions, the positions of the minimum and maximum IPR's both move towards lower disorder values when L increases. It seems plausible that they both go to zero in the limit of infinite system size, consistent with an extension of the localized regime down to infinitesimal disorder strength and the absence of a phase transition in two dimensions. However, the fact that the overall behavior in a finite system size in two and three dimensions is very similar, hints at the role of $d=2$ as a marginal dimension in the Anderson model.

A better insight into the behavior of the phase-space IPR can be gained by considering the position of the maxima, which shift to a smaller disorder strength with increasing system size, independently of the dimensionality. For a given system size L, the maximum phase-space IPR appears in the localized regime at a certain disorder strength W. Now, for a localized state at this fixed disorder strength, but at larger system size, the phase-space IPR becomes independent of the spatial structure once the width of the minimal uncertainty state (2) exceeds the localization length. In this regime, the phase-space IPR is dominated by momentum-space features. Since we know that $dP_k/dW<0$, we can conclude that $dP/dW<0$. Therefore, the maximum of $P(W)$ shifts to a smaller disorder strength when the system size is increased. Furthermore, from this argument it follows that in one and two dimensions the maximum shifts to $W=0$ in the limit $L\to\infty$ if we infer that all states are localized in the thermodynamic limit.

In order to discuss the position of the minimum IPR, we now turn to the ballistic regime at weak disorder. The coupling between plane waves within first order perturbation theory depends on two contrary effects. On the one hand, the number of plane waves into which scattering may occur increases with the system size. On the other hand, since the disorder potentials at different lattice sites are uncorrelated, the individual coupling matrix elements decrease with the size of the system. However, independently of the dimension the increased density of states dominates and scattering becomes more effective as the system size increases. This corresponds to a shrinking of the ballistic regime, which can be seen in Fig. 2 as a shift of the curves to smaller W with increasing L. This discussion, however, does not restrict the position of the minimum of P as a function of system size since the minimum always appears in the diffusive regime. Indeed, as Fig. 6 shows, with increasing L, the position of the minimum clearly shifts towards weaker disorder in two dimensions while it shifts to stronger disorder in three dimensions.

VII. CONCLUSIONS

In this study of the phase-space properties of the Anderson model, we have demonstrated the potential immanent to

this approach and, in particular, its advantages over approaches based purely on real or momentum-space properties. In contrast to the latter ones, the phase-space approach allows one to treat real and momentum space on the same footing. The well-studied Anderson model has allowed us to establish an interpretation of the phase-space IPR which will be useful in cases where no independent information is available.

We found that the crossover between the diffusive and the localized regimes is accompanied by an increase of the phase-space IPR which, in three dimensions, evolves to a sharp step in the thermodynamic limit. This is a signature of the Anderson metal-insulator transition.

The jump of the phase-space IPR at the Anderson transition implies a dramatic reorganization of the Husimi distribution from a large spread over phase space to localization not only in real space but also in phase space. This scenario is not only relevant for the $d=3$ Anderson model, but corresponds to the very similar one that was recently found for the Aubry-André model.[6] It is advantageous to exploit this similarity. The one-dimensional Aubry-André model allows for a direct visualization of the changes in the Husimi function at the metal-insulator transition. Furthermore, in numerical treatments of the Aubry-André model, the system size may be varied by more than two orders of magnitude, thus allowing for a much more detailed study of the phase transition.[25]

Moreover, by putting together the insights gained from phase space into the Aubry-André model and the Anderson model, a unified physical interpretation of the different dependencies on dimensionality emerges. In both cases, a potential-induced coupling of plane waves with distant momenta is required for a phase transition to occur. This mechanism explains the different critical dimensions in the two models.

It will be interesting to apply these phase-space concepts to interacting systems where the possibility to characterize individual many-particle states is expected to be of great value. Work along these lines is in progress.

ACKNOWLEDGMENTS

This work was supported by the Sonderforschungsbereich 484 of the Deutsche Forschungsgemeinschaft. D.W. thanks the European Union for financial support within the RTN program. The numerical calculations were carried out partly at the Leibniz-Rechenzentrum München.

[1] W. P. Schleich, *Quantum Optics in Phase Space* (Wiley-VCH, Berlin, 2001).
[2] K. Takahashi and N. Saitô, Phys. Rev. Lett. **55**, 645 (1985).
[3] T. Dittrich, P. Hänggi, G.-L. Ingold, B. Kramer, G. Schön, and W. Zwerger, *Quantum Transport and Dissipation* (Wiley-VCH, Weinheim, 1998), Chap. 6.
[4] N. F. Mott and W. D. Twose, Adv. Phys. **10**, 107 (1961).
[5] S. Aubry and G. André, Ann. Israel Phys. Soc. **3**, 133 (1980).
[6] G.-L. Ingold, A. Wobst, C. Aulbach, and P. Hänggi, Eur. Phys. J. B **30**, 175 (2002).
[7] B. Kramer and A. MacKinnon, Rep. Prog. Phys. **56**, 1469 (1993).
[8] A. Wehrl, Rep. Math. Phys. **16**, 353 (1979).
[9] B. Mirbach and H. J. Korsch, Phys. Rev. Lett. **75**, 362 (1995).
[10] D. Weinmann, S. Kohler, G.-L. Ingold, and P. Hänggi, Ann. Phys. (Leipzig) **8**, SI-277 (1999).
[11] A. Wobst, G.-L. Ingold, P. Hänggi, and D. Weinmann, Eur. Phys. J. B **27**, 11 (2002).
[12] E. Abrahams, P. W. Anderson, D. C. Licciardello, and T. V. Ramakrishnan, Phys. Rev. Lett. **42**, 673 (1979).
[13] M. Hillery, R. F. O'Connell, M. O. Scully, and E. P. Wigner, Phys. Rep. **106**, 121 (1984).
[14] K. Husimi, Proc. Phys. Math. Soc. Jpn. **22**, 264 (1940).
[15] K. E. Cahill and R. J. Glauber, Phys. Rev. **177**, 1882 (1969).
[16] G. Manfredi and M. R. Feix, Phys. Rev. E **62**, 4665 (2000).
[17] A. Sugita and H. Aiba, Phys. Rev. E **65**, 036205 (2002).
[18] D. J. Thouless, Phys. Rep. **13**, 93 (1974).
[19] M. Schreiber, J. Phys. C **18**, 2493 (1985).
[20] Y. Hashimoto, K. Niizeki, and Y. Okabe, J. Phys. A **25**, 5211 (1992).
[21] A. D. Mirlin, Phys. Rep. **326**, 259 (2000).
[22] I. Varga and J. Pipek, cond-mat/0204041, Phys. Rev. E (to be published).
[23] G.-L. Ingold, A. Wobst, C. Aulbach, and P. Hänggi, in *The Anderson Transition and its Ramifications – Localisation, Quantum Interference, and Interactions*, edited by T. Brandes and S. Kettemann, Lecture Notes in Physics (Springer, New York, 2003).
[24] A. MacKinnon and B. Kramer, Phys. Rev. Lett. **47**, 1546 (1981).
[25] C. Aulbach, G.-L. Ingold, A. Wobst, P. Hänggi, and I. Varga (unpublished).
[26] For certain states deviations from this result may occur due to the integral approximation, as for example in the case $\int_0^L dx \exp(2\pi i x)=0 \neq \Sigma_1^L \exp(2\pi i x)=L$. These states are of zero measure in the limit of large system size.
[27] Due to numerical limitations, the range of available system sizes in two and particularly in three dimensions is quite small. On the one hand, the system size should be sufficiently large compared to the width of the minimal uncertainty state (2) in order to avoid artifacts stemming from the periodic boundary conditions. On the other hand, the numerical efforts required in the diagonalization of the Hamiltonian (6) limit the system size from above.